Electronic Supplementary Material (ESI) for Nanoscale.

Supporting Information for

3D macroporous CUPC/g-C_3N_4 heterostructures for highly efficient multifunctional solar evaporation

Cong Chu, Zhikai Jia, Yu Yu, Kejian Ding and Songmei Wu*

School of Physical Science and Engineering, Beijing Jiaotong University, No. 3

Shangyuancun, Haidian District, Beijing 100044, P. R. China

1. Calculation of photothermal conversion efficiency in nanofluid

Calculation of the photothermal efficiency is based on the temperature at the dynamic thermal equilibrium and the temperature change during the cooling process. The photothermal conversion efficiency (η) is defined as follows:

$$\eta = \frac{Q_{in}}{A * S_M} \tag{S1}$$

where Q_{in} is the heat energy converted from light energy,

$$\sum(m_i c_i)\frac{dT}{dt} = Q_{in} - Q_{dis} \tag{S2}$$

where m_i is the mass of each component, c_i is the specific heat capacity of each component, Q_{dis} is the heat dissipation.

At the beginning of the irradiation, heat absorption is greater than heat dissipation, thus $\frac{dT}{dt}$ is larger than zero and the overall system temperature T(t) will rise.

$$Q_{dis} = h * A_{dis} * [T(t) - T_{am}] \tag{S3}$$

where A_{dis} is the heat dissipation area; T_{am} is the ambient temperature; T(t) is the instantaneous temperature and h is the heat transfer coefficient (in W m^{-2} °C^{-1})

As the temperature increases, the system loses more heat to the environment and therefore reaches dynamic equilibrium when $\frac{dT}{dt}$ equals zero. Then the system starts to cool down when the artificial light source is turned off.

$$\sum(m_i c_i)\frac{dT}{dt} = - Q_{dis} = - h * A_{dis} * [T(t) - T_{am}] \tag{S4}$$

By integrating the formula (S4), we have

$$\ln\frac{[T(t)-T_{am}]}{[T_{eq}-T_{am}]}=-\frac{h*A_{dis}}{\sum(m_ic_i)}*t \tag{S5}$$

where B is defined in the following equation

$$B=\frac{h*A_{dis}}{\sum(m_ic_i)} \tag{S6}$$

So that

$$\ln\frac{[T(t)-T_{am}]}{[T_{eq}-T_{am}]}=-B*t \tag{S7}$$

Overall, the photothermal conversion efficiency can be calculated:

$$\eta=\frac{[T_{eq}-T_{am}]*B*\sum(m_ic_i)}{A*S_M} \tag{S8}$$

where T_{eq} is equilibrium temperature; T_{am} is the ambient temperature; m_i is the sample mass; c_i is the specific heat capacity of the nanofluid; S_M is the irradiance (both 1100 W m^{-2}); A is the solar radiation area (the instrument used here is a test tube with an inner diameter of 1.9 cm and a solution height of 8.0 cm, and the estimated light area is about 23.9 cm^2).

2. Analysis of CUPC-CN composites

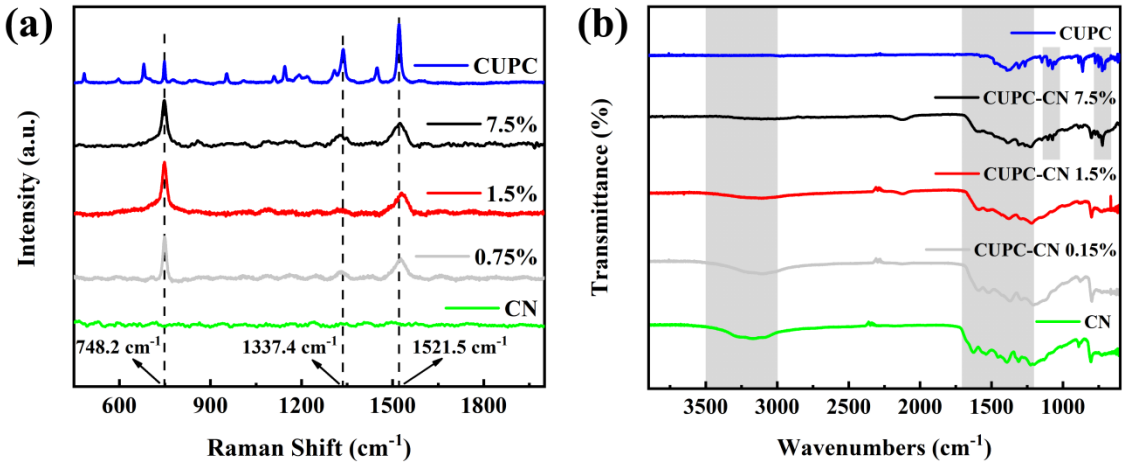

Figure S1. Raman spectra (a) and FTIR spectra (b) of pristine CN, CUPC and CUPC-CN composites.

In Raman spectra, slightly broadened CUPC bands at 748.2, 1337.4 and 1521.5 cm^{-1} can be clearly resolved in CUPC-CN composites. These bands were assigned to out-of-plane vibration of benzene, stretching of C−N−C bridge and Cu–N band, symmetric stretching vibration C–C bond in the pyrrole group, respectively[1, 2]. FTIR spectra in Figure S1 reveal that at low loading ratios of 0.15 and 1.5 wt%, the characteristic bands are dominated by pristine CN. However, the broad weak band around 3187 cm^{-1} smoothes down with increasing loading ratio of CUPC, indicating that the stretching of N−H units is suppressed by homogeneous adhesion of CUPC molecules on the surface of porous g-C_3N_4. With large loading ratio of 7.5 % , characteristic signals of CUPC appears obviously at 729 cm^{-1} and 1089 cm^{-1} owing to out-of-plane vibration of C−N band and in-plane vibration of C−N band and in-plane mode of pyrrole respectively[3-6] .

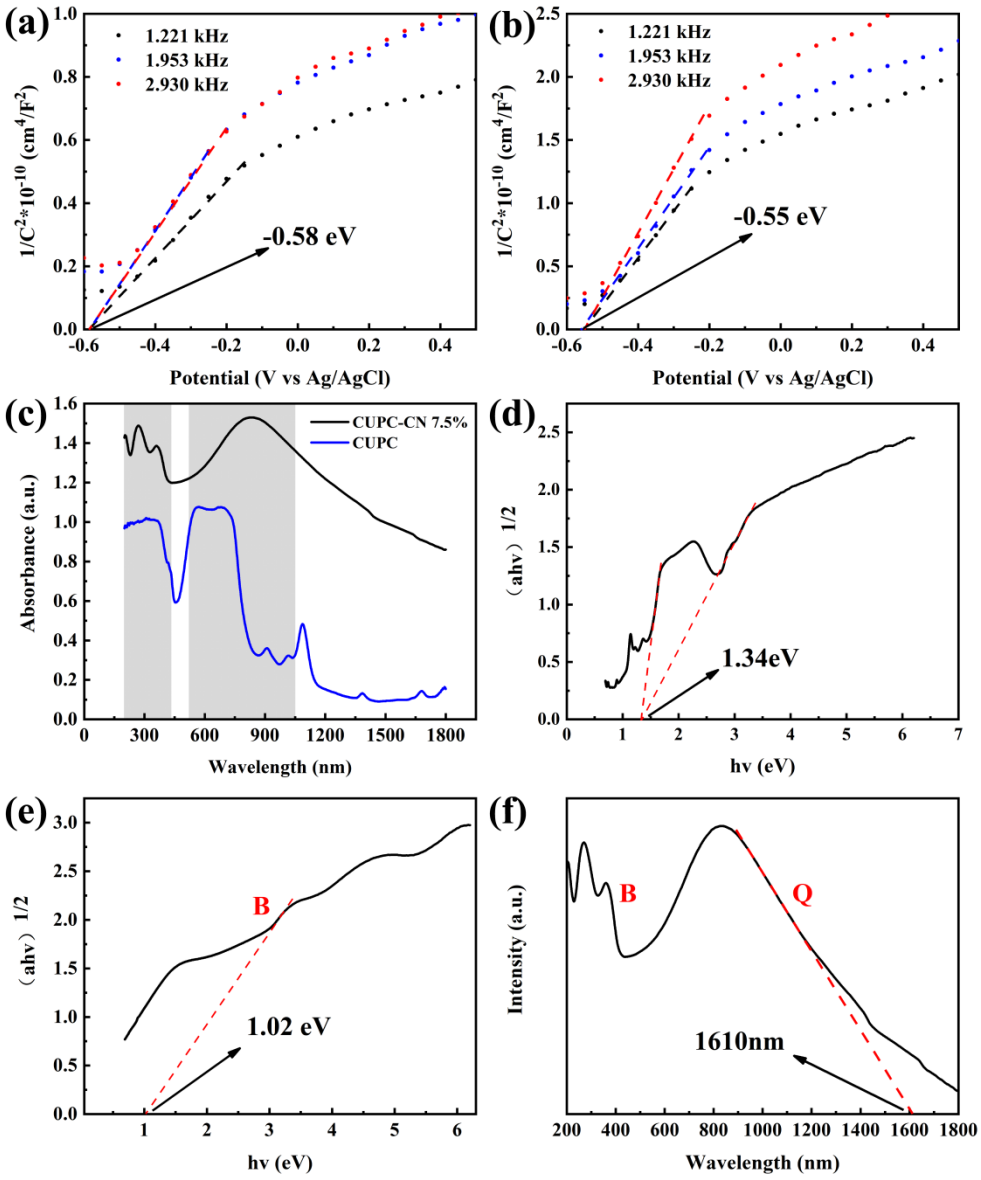

Figure S2. Band diagram analysis: Mott-Schottky curves for (a) CUPC and (b) CUPC-CN 7.5; (c) UV-vis absorption spectra of CUPC and CUPC-CN 7.5; Tauc plot diagram for (d) CUPC and (e) CUPC-CN 7.5; (f) Band gap evaluated by linear intercept method for CUPC-CN 7.5.

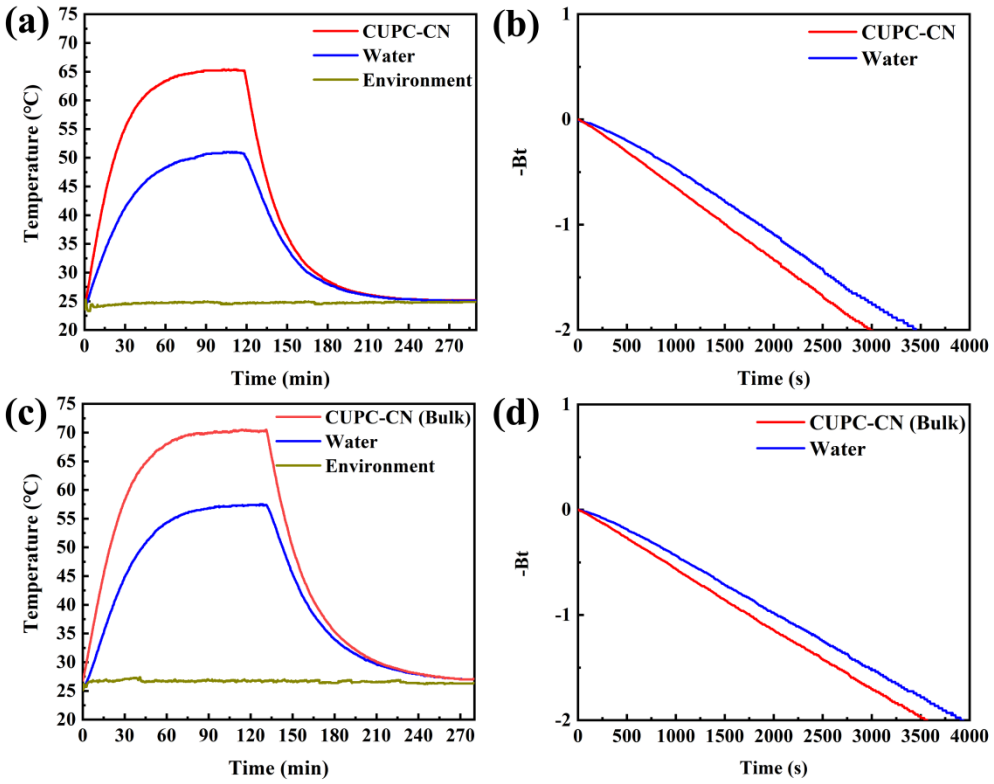

Figure S3. Photothermal conversion measurement in nanofluid by using macroporous and bulk CUPC-CN 1.5. Temperature change and Bt-value: (a) and (b) for macroporous CUPC-CN 1.5; (c) and (d) for bulk CUPC-CN 1.5.

3. Analysis of CUPC-CN membranes

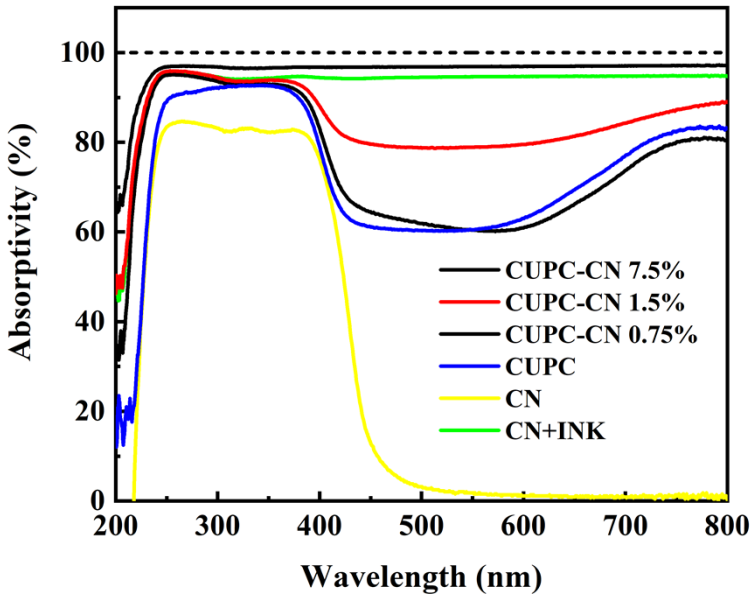

Figure S4. UV-Vis absorptivity of CN, CN+INK and CUPC-CN membranes.

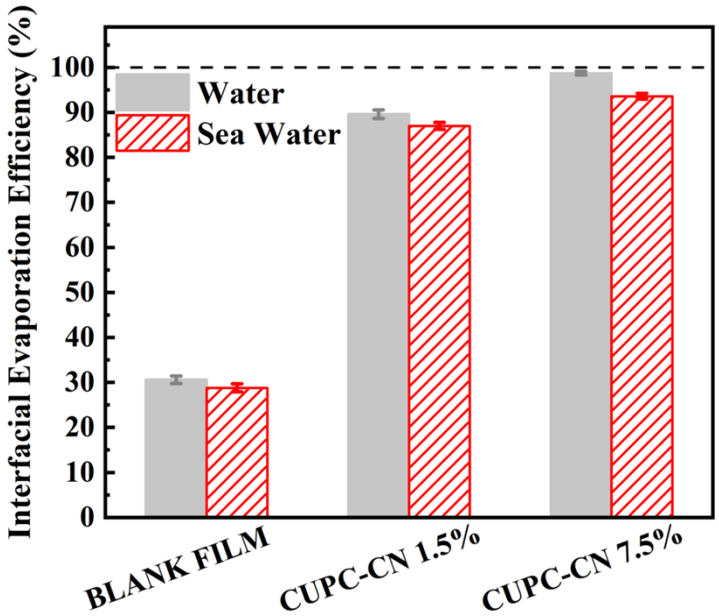

Figure S5. Interfacial evaporation efficiency of sea water and deionized water by using blank film and CUPC-CN composite membranes.

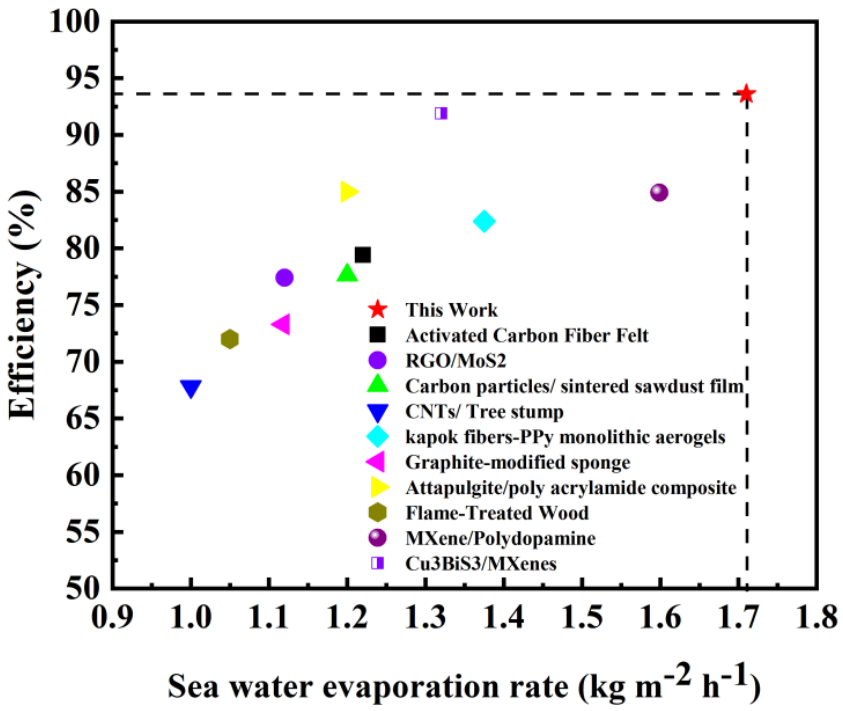

Figure S6. Comparison of sea water evaporation rate and efficiency with recent reported work under 1 kW m^{-2} illumination (Activated Carbon Fiber Felt, RGO/MoS_2[7], Carbon particles/sintered sawdust film[8], CNTs/ Tree stump[9], kapok fibers-PPy monolithic aerogels[10], Graphite-modified sponge[11], Attapulgite/poly acrylamide composite[12], Flame-Treated Wood[13], MXene/Polydopamine[14], Cu_3BiS_3/MXenes[15]).

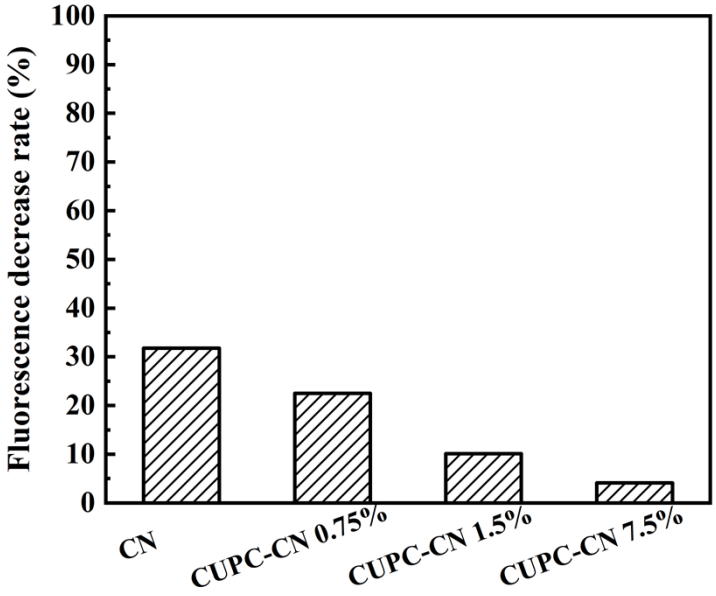

Figure S7. Fluorescence decrease rate of ROS indicator by adding the scavenger of superoxide free radical.

References

[1] J. Sun, J. Bian, J. Li, Z. Zhang, Z. Li, Y. Qu, L. Bai, Z.-D. Yang, L. Jing, Appl. Catal. B: Environ., 277 (2020).

[2] D. Li, Z. Peng, L. Deng, Y. Shen, Y. Zhou, Vib. Spectrosc., 39 (2005) 191-199.

[3] K.C. Christoforidis, Z. Syrgiannis, V. La Parola, T. Montini, C. Petit, E. Stathatos, R. Godin, J.R. Durrant, M. Prato, P. Fornasiero, Nano Energy, 50 (2018) 468-478.

[4] X. Chen, R. Shi, Q. Chen, Z. Zhang, W. Jiang, Y. Zhu, T. Zhang, Nano Energy, 59 (2019) 644-650.

[5] L. He, M. Fei, J. Chen, Y. Tian, Y. Jiang, Y. Huang, K. Xu, J. Hu, Z. Zhao, Q. Zhang, H. Ni, L. Chen, Mater. Today, 22 (2019) 76-84.

[6] R. Aroca, A. Thedchanamoorthy, Chem. Mater., 7 (1995) 69-74.

[7] X. Feng, J. Zhao, D. Sun, L. Shanmugam, J.-K. Kim, J. Yang, J. Mater. Chem. A, 7 (2019) 4400-4407.

[8] S. Liu, C. Huang, X. Luo, C. Guo, Appl. Energ., 239 (2019) 504-513.

[9] Y. Wang, H. Liu, C. Chen, Y. Kuang, J. Song, H. Xie, C. Jia, S. Kronthal, X. Xu, S. He, L. Hu, Adv. Sustain. Syst., 3 (2019).

[10] P. Mu, W. Bai, Y. Fan, Z. Zhang, H. Sun, Z. Zhu, W. Liang, A. Li, J. Mater. Chem. A, 7 (2019) 9673-9679.

[11] Z. Zhang, P. Mu, J. He, Z. Zhu, H. Sun, H. Wei, W. Liang, A. Li, ChemSusChem, 12 (2019) 426-433.

[12] J. Jia, W. Liang, H. Sun, Z. Zhu, C. Wang, A. Li, Chem. Eng. J., 361 (2019) 999-1006.

[13] G. Xue, K. Liu, Q. Chen, P. Yang, J. Li, T. Ding, J. Duan, B. Qi, J. Zhou, ACS Appl. Mater. Inter., 9 (2017) 15052-15057.

[14] Y. Jin, K. Wang, S. Li, J. Liu, J. Colloid Interf. Sci., 614 (2022) 345-354.

[15] Z. Wang, K. Yu, S. Gong, H. Mao, R. Huang, Z. Zhu, ACS Appl. Mater. Inter., 13 (2021) 16246-16258.